

Quantum splitting and its dynamics in GdLiF₄:Nd

W. Jia, Y. Zhou, S. P. Feofilov, and R. S. Meltzer

Department of Physics and Astronomy, University of Georgia, Athens, Georgia 30602, USA

J. Y. Jeong and D. Keszler

Department of Chemistry, 153 Gilbert Hall, Oregon State University, Corvallis, Oregon 97331-4003, USA

(Received 28 January 2005; revised manuscript received 20 April 2005; published 9 August 2005)

Efficient quantum splitting and sensitization of Gd³⁺ is demonstrated for the Gd³⁺-Nd³⁺ system in GdLiF₄:Nd 2%. The quantum splitting results from a two-step cross-relaxation energy transfer between Gd³⁺ and Nd³⁺ that first involves a transition ⁶G → ⁶I on Gd³⁺ and an excitation within the 4f³ configuration of Nd³⁺ followed by a second cross-relaxation energy transfer that brings Gd³⁺ to ⁶P_{7/2}. The excited Nd³⁺ ion rapidly relaxes, nonradiatively, to the emitting ⁴F_{3/2}. The excited Gd³⁺ ion then transfers its energy back to Nd³⁺, which gives rise to the second photon. The process is studied by emission and excitation spectroscopy. The result is a quantum yield for the emission of IR photons, which has its maximum of about 1.05 ± 0.35, at 175 nm. The dynamics of both the Gd³⁺ and Nd³⁺ excited states are studied in detail, providing information about the mechanisms and rates for the various energy transfer processes. It appears that the second step in the quantum splitting is less efficient than the first. It is found that energy migration among the Gd³⁺ ions plays an important role in the quantum splitting and that there is strong evidence that the exchange interaction is the dominant mechanism in the energy transfer. This system provides excellent insights into the quantum splitting process, especially with regard to an evaluation of the details of the dynamics.

DOI: [10.1103/PhysRevB.72.075114](https://doi.org/10.1103/PhysRevB.72.075114)

PACS number(s): 78.40.Ha, 71.70.Gm, 78.47.+p, 78.55.Hx

I. INTRODUCTION

It has been suggested that improvements in fluorescent lamps could be realized by replacing the mercury discharge by xenon, thereby removing the deleterious environmental impact of mercury and at the same time improving the energy efficiency. Such innovations require a phosphor that absorbs one vacuum ultraviolet (VUV) photon and emits two or more visible photons, an effect known as quantum splitting or downconversion.¹

Quantum splitting can occur either through a process of sequential cascade emission² as an excited ion returns to its ground state by first radiating to an intermediate state or by some cross-relaxation process that enables the initially excited ion to share its excitation energy with two or more ions, each of which emits a visible photon. Both of these processes have been demonstrated. Cascade emission was first demonstrated in YF₃:Pr with a 140% quantum efficiency.³ Cross-relaxation-induced quantum splitting has been described for GdLiF₄:Eu with an internal quantum efficiency of 190%.⁴

Unfortunately, neither of these schemes has so far yielded a useful phosphor. For the cascade emission, the first photon occurs at 406 nm too far in the deep blue, where the sensitivity of the human eye is very low. For the cross-relaxation scheme in GdLiF₄:Eu, the absorption of the VUV photon is too weak to produce a phosphor with high brightness.⁵

We attempted to sensitize the absorption by adding Nd³⁺ to GdLiF₄:Eu³⁺. We found that Nd³⁺ does effectively sensitize the excitation of Gd³⁺. However, in addition, Nd³⁺ undergoes its own very strong cross-relaxation with the Gd³⁺ system, producing efficient quantum splitting. A similar effect⁶ has recently been reported for GdLiF₄:Tm³⁺. In this paper we study, in detail, the quantum splitting process for

the singly doped system, GdLiF₄:Nd. The result of exciting Nd³⁺ into the 4f²5d state in the VUV is the appearance of two infrared photons. While this material will not be a commercially viable quantum splitting phosphor since the photons are in the infrared and because of the large energy loss, even if two photons were produced per input photon, it does provide important insights into the dynamics and mechanisms of the quantum splitting process. In this paper we (1) demonstrate the existence of the quantum splitting, (2) obtain the actual quantum efficiency of the system relative to the number of input VUV photons, (3) measure and analyze the dynamics of the processes using time-resolved emission, and (4) discuss the mechanisms for the energy transfer.

II. EXPERIMENT

Samples of GdLiF₄:Nd containing 1, 2, and 3 mol% Nd were prepared in powder form. GdF₃ was first synthesized by heating a mixture of 1 Gd₂O₃ (99.99%, Alfa Aesar) and 8 NH₄F (99.99%, Alfa Aesar) at 900 °C for 1.5 h. The resulting product was then mixed with 1.15 LiF (99.99%, Alfa Aesar), 0.01, 0.02, or 0.03 Nd₂O₃ (99.99%, Alfa Aesar), and 4 NH₄F (99.99%, Alfa Aesar) and thoroughly ground. The mixture was then fired at 750 °C for 1.5 h in a Pt crucible; the Pt crucible was covered and positioned inside an alumina crucible filled with activated carbon and NH₄F to limit the exposure of the sample to air.

All spectra were obtained at room temperature. Emission spectra were obtained by exciting the sample, contained in vacuum, with a deuterium lamp spectrally filtered with an Acton Model VM-502 VUV monochromator containing a concave grating so that selective excitation could be performed. The visible and UV emission was dispersed with an

Acton Spectrapro-150 spectrometer and was detected with a Santa Barbara Instrument Group Model ST-6I CCD camera at the exit focal plane. Emission spectra in the VUV were obtained by exciting the sample with a GAM Laser, Model EX5, pulsed molecular F₂ laser whose output is at 157 nm. The sample emission was focused onto the entrance slit of the VUV monochromator. The emission was detected with a solar blind PMT with a MgF₂ window located at a third slit of the VUV monochromator that was scanned to obtain the spectrum. All emission spectra were corrected for the wavelength-dependent response of the detection system. For cw excitation in the UV, a UV-enhanced Ar⁺ laser was used at 351 nm.

Excitation spectra were obtained by scanning the VUV monochromator, illuminated by the deuterium lamp, while detecting the emission with a PMT after passing the luminescence through appropriate colored glass or interference filters to select the desired components of the emission. Two PMT detectors were used, both having quartz windows yielding a response in the UV down to 200 nm. One (Hamamatsu R943) had a GaAs photocathode so that emission up to 900 nm could be measured. The other had a photocathode with an S-20 response. The excitation spectra of each sample were compared to that of a reference sample of sodium salicylate whose quantum efficiency is assumed to be about 58% and constant over the excitation wavelength range from 140 to 320 nm.⁷ The measured quantum yield is relative to input photons rather than absorbed photons since we have not obtained any reflectance measurements for either the samples or the reference. This assumes similar reflectivities of the sample and the sodium salicylate reference.

For the time-resolved data, the sample was excited with the pulsed laser at 157 nm (10 ns pulse width), while the emission was detected with the same PMTs described above for the excitation spectra. Temporal resolution was about 20 ns. The emission was selected with a 0.25 m monochromator and additional colored glass or interference filters to block light at other wavelengths from entering the monochromator. The bandwidth of the instrument was ~3 nm. The main limitations of the time-resolved spectra were extraneous signals at early times coming either from broadband red/NIR emission from atomic fluorine in the laser discharge or from fast decay of defect centers that were excited by the VUV excitation. This red/NIR emission was so strong that it was very difficult to do any time-resolved spectroscopy from about 620 to 750 nm. For direct excitation of the 4f³ states of Nd³⁺, the third harmonic of a pulsed Nd:YAG laser at 355 nm (10 ns pulse width) was utilized.

III. DEMONSTRATION OF QUANTUM SPLITTING

In Fig. 1 the emission spectrum is presented for two different excitation wavelengths, 351 and 160 nm. The emission from 200 to 950 nm is dominated by the ⁴F_{3/2} → ⁴I_{9/2} transition. However, emission from the ⁴D_{3/2} and ²P_{3/2} states of Nd³⁺ is also observed. Weak emission from the ⁶P_{7/2} state of Gd³⁺ is observed at 313 nm. While it is not evident in this time-averaged spectrum, emission occurs at 281 nm from the ⁶I state of Gd³⁺. Emission from the 4f²5d state of Nd³⁺ in the

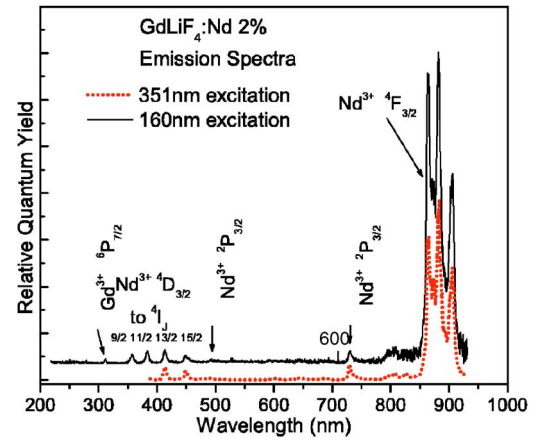


FIG. 1. (Color online) Relative quantum yield of GdLiF₄:Nd2% exciting at 160 nm (black, solid curve) and at 351 nm (red, dashed curve). The spectra are normalized on the Nd³⁺⁴D_{3/2} and ²P_{3/2} quantum yields.

wavelength range of 180 to 270 nm, which dominates the spectrum of YLiF₄:Nd,⁸ is not observed in GdLiF₄:Nd, suggesting efficient energy transfer from Nd³⁺ to Gd³⁺, i.e., strong sensitization.

When the spectra excited at the two different wavelengths are compared, by normalizing to the ⁴D_{3/2} and ²P_{3/2} emission, it is seen that under 160 nm excitation, the relative intensity of the ⁴F_{3/2} emission is more than double that observed for 351 nm excitation. This suggests a process that enhances the excitation of ⁴F_{3/2} in a manner that was used to identify quantum splitting for GdLiF₄:Eu.⁴ This is just the cross-relaxation process responsible for quantum splitting.

The processes are illustrated in Fig. 2. The diagram shows

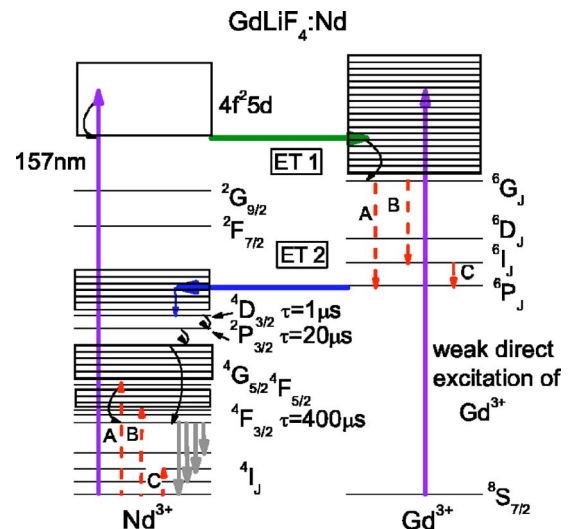


FIG. 2. (Color online) Energy level diagrams of Nd³⁺ and Gd³⁺ in GdLiF₄:Nd with the relevant energy levels labeled. The open box represents the 4f²5d band of Nd³⁺. The boxed areas with horizontal lines represent energy regions with a high density of 4fⁿ levels. ET1 and ET2 indicate resonant energy transfer processes. Labels A, B, and C next to the red (dashed) lines denote three cross-relaxation energy transfer processes. Some of the intrinsic lifetimes are indicated.

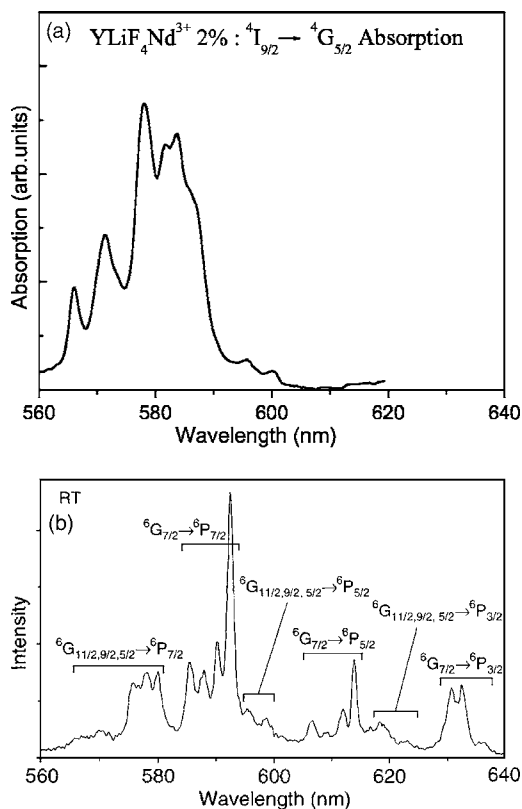


FIG. 3. (a) Absorption spectrum of YLiF₄:Nd2% and (b) the emission spectrum of YLiF₄:Gd5% (Ref. 9) showing significant spectral overlap.

the relevant $4f^3$ and $4f^7$ energy levels of Nd³⁺ and Gd³⁺, respectively. Boxed regions with horizontal lines indicate a high density of states of the two $4f^n$ configurations for which rapid multiphonon relaxation occurs. The open box represents the $4f^25d$ band of Nd³⁺. The $4f^65d$ band of Gd³⁺ is off the energy scale and is not relevant here. The long vertical arrow represents the VUV excitation of Nd³⁺ into the $4f^25d$ band. Rapid energy transfer to a nearly resonant $4f^7$ state of Gd³⁺, labeled by ET 1, followed by rapid nonradiative relaxation, populates the 6G_J states of Gd³⁺. Cross-relaxation energy transfer from the ${}^6G_{7/2}$ state of Gd³⁺ can occur via two paths. One of these, indicated by the red (dashed) arrows labeled A on the energy level diagrams of Gd³⁺ and Nd³⁺, results in a transition ${}^6G_{7/2} \rightarrow {}^6P_J$ on Gd³⁺, as has been previously observed in the Gd-Eu couple, with a simultaneous ${}^4I_{9/2} \rightarrow {}^4G_{5/2}$ excitation on Nd³⁺. These two transitions have considerable overlap, as shown in the room-temperature spectra of Fig. 3, where the ${}^6G_J \rightarrow {}^6P_J$ emission of Gd³⁺ observed⁹ in YLiF₄:Gd is compared to the ${}^4I_{9/2} \rightarrow {}^4G_{5/2}$ absorption of YLiF₄:Nd. Subsequently, rapid multiphonon relaxation leads to feeding of the ${}^4F_{3/2}$ metastable state from which strong IR emission occurs.

The second pathway involves a transition ${}^6G_{7/2} \rightarrow {}^6I_J$ on Gd³⁺ coupled with a ${}^4I_{9/2} \rightarrow {}^4F_{5/2}$, ${}^2H_{9/2}$, or ${}^4F_{7/2}$ transition on Nd³⁺, as indicated by the red (dashed) arrows labeled B in Fig. 2. Although the spectra are not available for comparison, the transition energies for Nd³⁺ in the absorption¹⁰ and Gd³⁺ predicted for emission⁶ are likely to have good resonances.

In addition, Peijzel *et al.*⁶ have shown that the reduced matrix elements for this second pathway are about an order of magnitude greater than for the first, making this process about two orders of magnitude faster under the similar resonance conditions. Indeed, as will be shown from studies of the dynamics, the pathway involving the 6I_J levels does dominate the cross-relaxation from ${}^6G_{7/2}$. However, 6I_J can further relax to 6P_J via another cross-relaxation process, shown by the red (dashed) arrows labeled C in Fig. 2, that excites the ${}^4I_{13/2}$ state of Nd³⁺. Evidence for this also exists from the dynamical studies discussed below.

The 6P_J states of Gd³⁺ then transfer their energy to the nearly resonant $4f^3$ states of Nd³⁺, as shown by the blue (solid) arrow labeled ET 2. Above the ${}^4D_{3/2}$ state of Nd³⁺ there is a very dense, almost continuous forest of energy levels from the $4f^3$ configuration among which the ${}^2L_{17/2}$ at $\sim 32\,000$ cm⁻¹ is in closest resonance with the ${}^6P_{7/2}$ states of Gd³⁺.¹⁰ Once excited, these will relax almost immediately to the ${}^4D_{3/2}$ level, which lives long enough to produce observable emission. Its decay, whose lifetime is about 1 μ s, is dominated by nonradiative relaxation to the ${}^2P_{3/2}$ level, which lives much longer with a lifetime of ~ 20 μ s. These and subsequent multiphonon relaxations ultimately feed the ${}^4F_{3/2}$ level, leading to the emission of a second IR photon. On the other hand, when the ${}^4D_{3/2}$ state is excited directly at 351 nm, the cross-relaxation step is eliminated so that the relative intensity of ${}^4F_{3/2}$ emission is less than half that obtained under 157 nm excitation. As described by Wegh *et al.*⁴ for GdLiF₄:Eu, this is strong evidence for quantum splitting. The dynamics of the system described below will provide further supporting evidence.

Finally, it should be noted that the assumption that the initial Nd³⁺ \rightarrow Gd³⁺ energy transfer (ET1 in Fig. 2) occurs to Gd³⁺ states resonant with the $4f^25d$ state of Nd³⁺ may not be a good one. Many possible cross-relaxation energy transfer processes are equally possible. These could excite many of the lower-lying states of Gd³⁺ below the energy of the $4f^25d$ state of Nd³⁺ ($\sim 56\,000$ cm⁻¹), shown on the Gd³⁺ energy level diagram as the boxed area with many horizontal lines in Fig. 2. For example, cross-relaxation processes could leave Nd³⁺ in the 4I_J levels $J=11/2, 13/2, 15/3$, and Gd³⁺ in states above 6G_J that conserve the total energy. Note that rapid multiphonon relaxation would still lead to a buildup in the population of the 6G_J levels of Gd³⁺, as had been assumed. Cross-relaxation processes are also possible in which the energy transfer would result in Gd³⁺ being excited to 6D_J , 6I_J , or 6P_J by leaving Nd³⁺ in its ${}^4F_{9/2}$ (14 800 cm⁻¹), ${}^4G_{7/2}$ (19 000 cm⁻¹), or ${}^4G_{11/2}$ (21 400 cm⁻¹) states, respectively. However, these processes would also still lead to quantum splitting since multiphonon relaxation would populate ${}^4F_{3/2}$ and the excited Gd³⁺ ion would still be capable of transferring its energy to Nd³⁺ for producing the second photon. These processes would supplement the energy transfer processes labeled as A and B that were previously discussed.

IV. EXCITATION SPECTRUM AND QUANTUM YIELD

The excitation spectra, detecting the ${}^4F_{3/2} \rightarrow {}^4I_{9/2}$ emission of Nd³⁺ at 780–910 nm, is shown in Fig. 4 for the 1% and

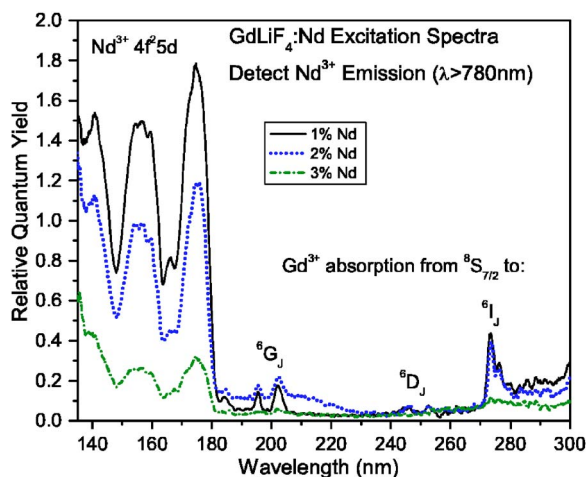


FIG. 4. (Color online) Excitation spectrum of GdLiF₄ containing 1, 2, and 3% Nd³⁺ and detecting the Nd³⁺⁴F_{3/2} emission using a cutoff filter that transmits for $\lambda > 780$ nm. Features of the ⁶G_J, ⁶D_J, and ⁶I_J levels of Gd³⁺ and the 4f²5d bands of Nd³⁺ are indicated.

2% and 3% Nd samples. It contains features associated both with Gd³⁺ and Nd³⁺, as indicated in the figure. One clearly sees the states of the 4f⁷ configuration of Gd³⁺, namely ⁶G_J, ⁶D_J, and ⁶I_J, indicating that the energy transfer between Gd³⁺ and Nd³⁺ occurs, as expected. The 4f²5d bands of Nd³⁺ are also clearly observed.

The quantum yield relative to that of the reference, sodium salicylate, achieves a maximum of 1.8 in the 2% Nd sample for excitation into the 4f⁷→5d bands of Nd³⁺ at 175 nm. This value is obtained by applying a number of corrections to the raw data. First, the raw data are corrected for the fact that the relative quantum efficiency of the PMT for the ⁴F_{3/2}→⁴I_{9/2} emission wavelength of Nd³⁺ between 860 and 910 nm is much less than that at the 380–460 nm emission wavelength range of sodium salicylate. A correction factor for the relative response of the PMT is obtained by convoluting the corrected emission of the sample and sodium salicylate reference, each with the quantum efficiency of the PMT, and calculating the ratio of these products yielding a correction factor of 20±6. A great deal of effort was made to accurately obtain the relative quantum efficiency of the PMT which, because of the rapid decrease in response in the region above 860 nm, leaves this considerable uncertainty of about ±30%. Second, it is estimated that only 33% of the ⁴F_{3/2} emitted photons occur on the ⁴F_{3/2}→⁴I_{9/2} transition, based on reported¹¹ emission spectra of YLiF₄:Nd and calculations of the branching ratios determined by a Judd-Ofelt analysis,¹² implying a further correction of about 3. An actual measurement of the branching ratios obtained from the IR emission spectrum was performed by Rufus Cone using an Applied Detector Corp. 403L Ge detector at the exit slit of a Spex 1000M spectrometer. All spectra were referenced against a tungsten halogen lamp operating at 2800 K. The measurement yielded a value of 31.1% for the fraction of the emission occurring to ⁴I_{9/2}, very close to the value calculated. The result was a correction factor of 3.22±0.3. Finally, there is an uncertainty concerning the relative reflectivities of the samples and sodium salicylate reference. Although these

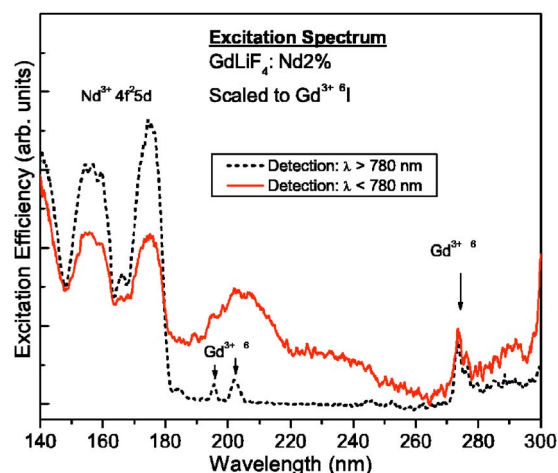


FIG. 5. (Color online) A comparison of the excitation spectra of GdLiF₄:Nd2% detecting only the ⁴F_{3/2} emission with $\lambda_{\text{detect}} > 780$ nm with that of the case of detection for $\lambda_{\text{detect}} < 780$.

may be somewhat different, they are probably both less than 20% in the strongly absorbing regions of the spectrum of interest. Thus, this should add not more than a ±10% error. Using an estimate that the absolute quantum yield of sodium salicylate as 0.58, implies an absolute quantum yield for the ⁴F_{3/2} emission of about 1.05±0.35. The estimated uncertainty is based on the accumulated errors discussed above. This value for the quantum yield is about three times the value of 0.32⁵ obtained for GdLiF₄:Eu. However, it is still well below the theoretical maximum quantum yield of 2 based on the quantum splitting scheme described above. This highlights the fact that even in a system that exhibits highly efficient quantum splitting, other losses can limit the absolute quantum yield. Indeed, measurements of the quantum efficiency of the GdLiF₄:Eu quantum splitting phosphor⁵ show that a broad defect absorption reduces the quantum efficiency considerably. A study of the dynamics will allow for an examination of some of the reasons for the reduced quantum yield for GdLiF₄:Nd.

The excitation spectra for detection above and below 780 nm are compared in Fig. 5. The spectra are normalized to the Gd³⁺⁶I transition. The black (dotted) curve is obtained detecting wavelengths $\lambda > 780$ nm so that only the Nd³⁺ IR emission from ⁴F_{3/2} is monitored. The red (solid) curve is the excitation spectrum for $\lambda < 780$ nm and is dominated by Nd³⁺ emission from ⁴D_{3/2}, which is not enhanced by the quantum splitting. Both the ⁶G excitation features of Gd³⁺ and the 4f²5d bands of Nd³⁺ are enhanced when detecting the ⁴F_{3/2} emission, supporting the conclusion that quantum splitting plays an important role in the emission. For detection with $\lambda < 780$ nm, there is evidence for an impurity or defect absorption band near 200 nm.

V. DYNAMICS OF THE QUANTUM SPLITTING

Despite the fact that a great deal of work has been done on quantum splitting due to cross-relaxation energy transfer (CRET), there have been, to our knowledge, only two studies,^{13,14} of the dynamics of this process. The studies con-

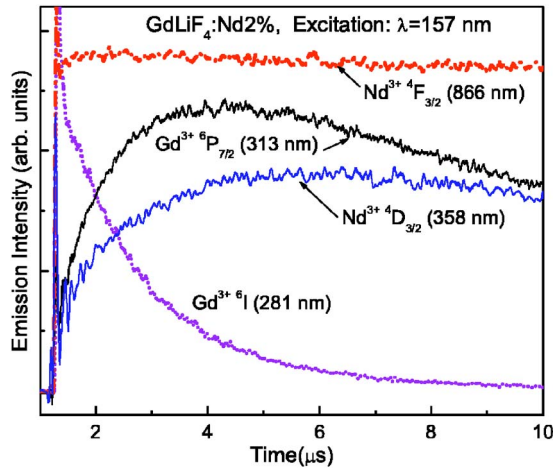


FIG. 6. (Color online) Time evolution of the 6I (281 nm) and ${}^6P_{7/2}$ (313 nm) emission intensities of Gd^{3+} and the ${}^4D_{3/2}$ and ${}^4F_{3/2}$ emission intensities of Nd^{3+} in a $GdLiF_4:Nd2\%$ sample under 157 nm pulsed laser excitation.

sidered the $Gd^{3+}-Eu^{3+}$ couple in $GdNaF_4:Eu^{3+}$ and in $GdLiF_4:Eu^{3+}$. Both the cross-relaxation and direct transfer were observed with rates about two orders of magnitude slower than for the $Gd^{3+}-Nd^{3+}$ couple studied here. As pointed out in Wegh *et al.*,⁴ the process achieves its efficiency because of energy migration among the Gd^{3+} ions that are stoichiometric in all known successful cross-relaxation energy transfer quantum splitters. Dipole-dipole energy transfer or exchange is just too slow except for ions that are near neighbors. The fact that energy migrates within the Gd^{3+} ions ensures that the excitation in the 6G_J levels of Gd^{3+} gets to spend a portion of its time as a near neighbor of Nd^{3+} . Thus the dynamics within the Gd^{3+} system is expected to play an important role in the process.

When a sample of $GdLiF_4$ containing 2% Nd^{3+} is excited at 157 nm with a molecular F_2 laser, one sees a buildup of the ${}^6P_{7/2}$ transition of Gd^{3+} at 313 nm, as shown in Fig. 6 by the black (dark solid) curve. This buildup has two components. One is very fast, at a rate that exceeds the time resolution of these experiments (<50 ns, limited by some background scattered light from the laser discharge and defect luminescence), which represents about 20% of the population feeding. The second is a slower buildup over several microseconds, representing about 80% of the feeding. The cause of these two components becomes clear from the dynamics of the 6I emission of Gd^{3+} at 281 nm shown by the purple (dotted) curve in Fig. 6. Its decay rate coincides with the ${}^6P_{7/2}$ population buildup rate. Also shown in Fig. 6 by the red (dot-dashed) curve is the emission at 866 nm from the ${}^4F_{3/2}$ state of Nd^{3+} , which also builds up within the temporal resolution of the experiment. Thus we conclude, as suggested based on an earlier discussion of the reduced matrix elements, that cross-relaxation process B from Fig. 2 is the dominant one in the quantum splitting. However, the fact that the ${}^6P_{7/2}$ population does have a very fast component indicates that there may also be a contribution from the cross-relaxation energy transfer process labeled A in Fig. 2. The relaxation of Gd^{3+} from 6I to 6P in a few microseconds is

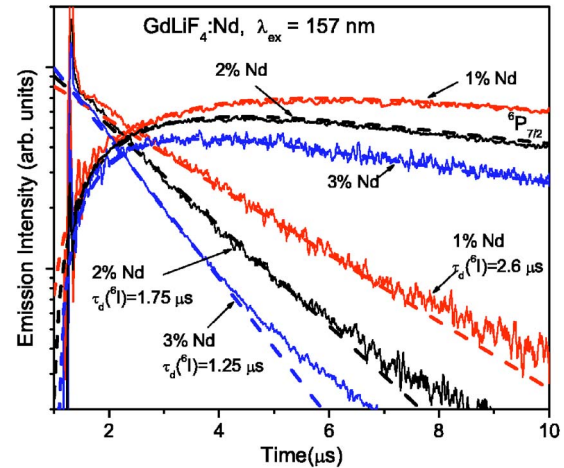


FIG. 7. (Color online) Time evolution of the 6I (281 nm) and ${}^6P_{7/2}$ (313 nm) emission intensities of Gd^{3+} under 157 nm pulsed excitation in $GdLiF_4:Nd$ for 1%, 2%, and 3% Nd concentrations. The dashed lines show the fits using the 6I decay times shown in the figure. Those same times are used as the rise times in the fits to the ${}^6P_{7/2}$ emission for the sample with the same Nd^{3+} concentration.

unlikely to occur due to multiphonon relaxation because of the large energy gap (~ 3000 cm^{-1}) and low phonon energies of the $GdLiF_4$ host, but rather most likely occurs through the cross-relaxation energy transfer process labeled C in Fig. 2. Consistent with this suggestion is the fact that the relaxation is dependent on Nd^{3+} concentration, as discussed below. In this process a Nd^{3+} ion is excited from the ${}^4I_{9/2}$ ground manifold to ${}^4I_{13/2}$, for which there is a good resonance match with the ${}^6I \rightarrow {}^6P$ transitions on Gd^{3+} .

The behavior of the dynamics of process C and its concentration dependence provides important information on the role of donor-donor energy transfer among the Gd^{3+} ions. The dynamics of the 6I and 6P emissions are shown as a function of concentration in Fig. 7. The relaxation process is nearly exponential, as seen by the dashed lines plotted over the 6I time-resolved emission that are fits to the data, assuming an exponential decay of 6I . The values for the fit are shown in the figure and are summarized in Table I. The relaxation rate scales nearly linearly with concentration, as expected. Also shown are the time-resolved intensity of the ${}^6P_{7/2}$ emission along with fits to the data using the 6I decay time as the feeding term in the ${}^6P_{7/2}$ population. Indeed, the same times describe both the 6I and ${}^6P_{7/2}$ emissions. The decay of ${}^6P_{7/2}$ is also nearly exponential with a rate that depends on the Nd^{3+} concentration. These rates are also summarized in Table II. The nearly exponential relaxation processes for all three concentrations suggests that energy migration among the Gd^{3+} ions is fast compared to these CRET relaxation rates. In that case the Gd^{3+} excitation samples all sites thereby spending a fraction of its time nearby a Nd^{3+} ion with which it can undergo CRET. If, after energy transfer from the $4f^25d$ state of Nd^{3+} to Gd^{3+} , the energy remained localized on that Gd^{3+} ion, the CRET rates would be highly nonexponential. In addition, without energy migration, CRET process C would be hindered, as all of the energy resonances that we have discussed assume that the Nd^{3+} ions

TABLE I. Experimental energy transfer rates.

Process	Nd ³⁺ conc.	Gd ³⁺	Nd ³⁺	Expt ET rate(s ⁻¹)
CRET A	All	⁶ G → ⁶ P	⁴ I _{9/2} → ⁴ G _{5/2}	> 2 × 10 ⁷
CRET B	All	⁶ G → ⁶ I	⁴ I _{9/2} → ⁴ F _{5/2} , ² H _{9/2}	> 2 × 10 ⁷
CRET C		⁶ I → ⁶ P	⁴ I _{9/2} → ⁴ I _{13/2}	
	1%			3.8 × 10 ⁵
	2%			5.7 × 10 ⁵
	3%			8.0 × 10 ⁵
Gd ³⁺ → Nd ³⁺		⁶ P _{7/2} → ⁸ S _{7/2}	⁴ I _{9/2} → ² L _{17/2}	
	1%			4.3 × 10 ⁴
	2%			6.7 × 10 ⁴
	3%			9.1 × 10 ⁴

are in their ground state. However, processes A and B leave the Nd³⁺ ion in an excited state for a time roughly equal to the lifetime of the ⁴F_{3/2} state of about 400 μs. Also, in the absence of rapid Gd³⁺-Gd³⁺ energy transfer, some of the possible processes providing the initial Nd³⁺ → Gd³⁺ energy transfer could also leave Nd³⁺ in an excited state, as discussed earlier, compromising the CRET processes A and B, which also assume that the Nd³⁺ ions are in their ground state.

The excited Gd³⁺ ions in the ⁶P_{7/2} state then undergo energy transfer to the nearly resonant 4f³ states of Nd³⁺ at a rate described by the decay of the Gd³⁺⁶P_{7/2} emission. Proof of this second step is seen by monitoring the ⁴D_{3/2} emission under 157 nm excitation. It is observed that this emission closely follows the Gd³⁺⁶P_{7/2} population with a small delay and that it has zero population immediately after the laser excitation (see Fig. 6). This occurs because the intrinsic ⁴D_{3/2} lifetime (~1 μs due to multiphonon relaxation to ²P_{3/2}) is much shorter than the ⁶P_{7/2} lifetime, as seen from its decay under direct 355 nm excitation into the 4f³ states just above ⁴D_{3/2}, as shown in Fig. 8. The fact that the ⁴D_{3/2} population closely follows the excited Gd³⁺ population demonstrates that energy transfer from Gd³⁺ to Nd³⁺ does occur, a process that is necessary for the second step of the quantum splitting process. The observation that the ⁴D_{3/2} emission (spectrally integrated) is more than an order of magnitude greater than the Gd³⁺⁶P_{7/2} emission (see Fig. 1) indicates that a significant fraction of the Gd³⁺ ions transfer their energy to Nd³⁺, since the two populations follow one another because of the short inherent lifetime of ⁴D_{3/2}. Its greater time-integrated intensity results from its faster radiative rate than that of ⁶P_{7/2}, which is spin forbidden. Since we do not know the relative radiative rates, it is not possible to estimate from these relative intensities the efficiency of this Gd³⁺ → Nd³⁺ energy transfer.

The ⁴D_{3/2} state decays nonradiatively to ²P_{3/2}, whose population dynamics is also shown in Fig. 8 for both 355 and 157 nm excitation. Under 355 nm excitation, it builds up at the ⁴D_{3/2} decay rate and decays in 20 μs, its intrinsic nonradiative lifetime. Under 157 nm excitation, it has a slower buildup, resulting from the population feeding from ⁴D_{3/2} whose population is controlled by energy transfer from ⁶P_{7/2} of Gd³⁺. The ²P_{3/2} decay ultimately feeds ⁴F_{3/2} through mul-

tiphonon relaxation down the ladder of states of Nd³⁺ from whose radiative decay provides the second photon in the quantum splitting arises. Thus, the feeding of ⁴F_{3/2} for the second step in the quantum splitting continues for ~100 μs.

The temporal behavior of the ⁴F_{3/2} emission further supports the presence of quantum splitting. As shown in Fig. 9, when the 4f³Nd³⁺ states just above ⁴D_{3/2} are excited directly at 355 nm, such that there is no quantum splitting, the ⁴F_{3/2} emission builds up with a rise time that is close to the value of the decay time of the ²P_{3/2}Nd³⁺ emission (20 μs). The ⁴F_{3/2} emission under 157 nm excitation, also shown in Fig. 9, shows a much more rapid buildup, as expected, due to the first step in the quantum splitting, namely the cross-relaxation step. However, note that the ⁴F_{3/2} emission does not immediately begin an exponential decay. Rather its population remains high due to feeding from the second step in the quantum splitting, which maintains a feeding term for about ~100 μs as ²P_{3/2} decays.

Attempts to fit the dynamics presented in Fig. 9 (dashed curves) with an exponential rise and decay indicate that under 355 nm excitation, the ⁴F_{3/2} emission has both a fast

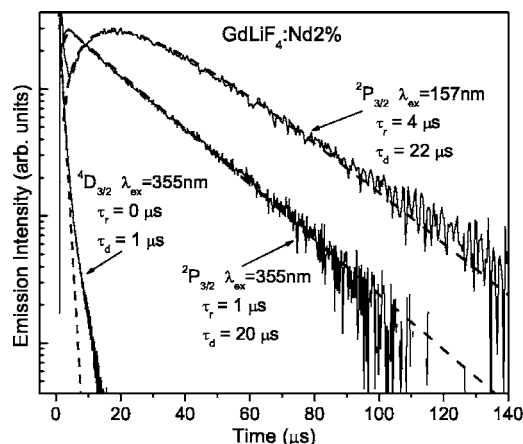


FIG. 8. Time evolution of the ⁴D_{3/2} and ²P_{3/2} emission of Nd³⁺ in a sample of GdLiF₄:Nd2% under 355 nm excitation and the ⁴P_{3/2} emission under 157 nm excitation. The decay of ²P_{3/2} is the rate-limiting state in the feeding of ⁴F_{3/2}. Also plotted as dashed lines are fits to the data using the rise and decay times indicated in the figure.

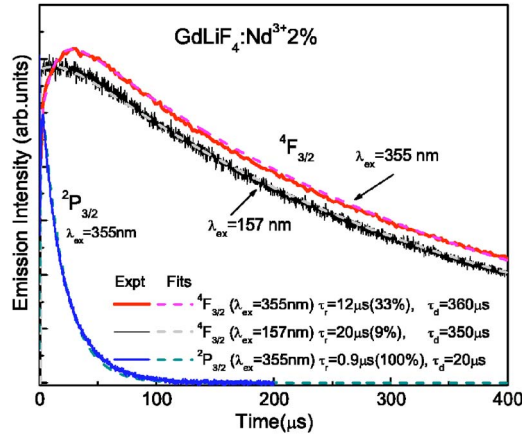


FIG. 9. (Color online) Time evolution of the ${}^2P_{3/2}$ and ${}^4F_{3/2}$ emission in a GdLiF₄:Nd2% sample under 355 and 157 nm excitation. The fits shown in the figure are obtained using the rise and decay times indicated in the legend. They percentage indicates the fraction of population buildup that is contributed by this rise time. The remainder of the population buildup is taken to appear immediately after excitation.

(immediate with respect to the experimental time resolution) followed by an exponential rise with a 12 μ s rise time. The latter represents only 33% of the total contribution to the feeding of the ${}^4F_{3/2}$ population. The source of the fast component is unknown, but it suggests the existence of some other channel of relaxation for 355 nm excitation. Under 157 nm excitation there is again a fast component, resulting from the first CRET step due to processes A and B, followed by an additional feeding through ${}^2P_{3/2}$ for about 100 μ s (see Fig. 8). Here the additional feeding contributes only 9% to the ${}^4F_{3/2}$ population. Under ideal conditions of quantum splitting, this should represent 50% of the contribution to the ${}^4F_{3/2}$ population through the process labeled ET 2 in Fig. 2. Because of the observation that even under 355 nm excitation there exists an unexplained very fast component to the ${}^4F_{3/2}$ population, it may be that a somewhat lower value than 50% should be expected. However, the fact that it is only 9% seems to explain, in part, the less than ideal quantum yield.

There are a number of potential sources for this reduced contribution, including radiative transitions from ${}^4D_{3/2}$ and ${}^2P_{3/2}$ that are observed in Fig. 1, radiative transitions from ${}^6P_{7/2}$ of Gd³⁺ prior to the energy transfer to Nd³⁺, the transfer of energy from ${}^6P_{7/2}$ of Gd³⁺ to impurities or defects, and cross-relaxation among Nd³⁺ ions. In addition, nonradiative processes involving ${}^4F_{3/2}$ are possible. Indeed, the observed lifetimes of the ${}^4F_{3/2}$ emission are below the low concentration limit of 535 μ s in GdLiF₄:Nd,¹⁵ and, in agreement with the results of Zhang *et al.*,¹⁵ the 2% and 3% samples exhibit significant nonexponential behavior indicative of Nd³⁺-Nd³⁺ cross-relaxation (not shown). However, while this would contribute to the reduced quantum yield, it would not explain the lower than expected contribution to the feeding of ${}^4F_{3/2}$.

VI. DISCUSSION

It is of interest to examine the mechanisms for the cross-relaxation energy transfer (CRET) responsible for the quan-

tum splitting. For closely spaced ion pairs, this may occur by dipole-dipole interactions or exchange interactions.¹⁶ For more distant pairs, the exchange will become unimportant because of its rapid decrease with distance. According to Forster-Dexter dipole-dipole energy transfer theory, the transfer rate, P_{AB}^{dd} can be written¹⁷ as

$$P_{AB}^{dd} = 1.4 \times 10^{24} f_A f_B S_{AB} \Delta E^{-2} R^{-6}. \quad (1)$$

Here f_A and f_B are the oscillator strengths of the transitions on Nd³⁺ and Gd³⁺, ΔE is the transition energy of each ion (in eV), R is the distance between the two ions (in Angstroms), and S_{AB} is the spectral overlap (in cm⁻¹) of the downward and upward transitions. In Fig. 3 it was shown for CRET process A that there are many ${}^4I_{9/2} \rightarrow {}^4G_{5/2}$ transitions of Nd³⁺ that are nearly resonant with the ${}^6G_J \rightarrow {}^6P_J$ transitions of Gd³⁺. The oscillator strength of each of these crystal field transitions of Nd³⁺ in YLiF₄ are typically¹⁰ about $\sim 5 \times 10^{-7}$, based on the spectral analysis of some of the individual crystal field transitions at 20 K. However, one can also estimate the oscillator strengths from experimental and calculated values integrated over all transitions in the manifolds by dividing by the number of final states, which yields about the same average oscillator strength per crystal field transition.¹⁸ A similar situation holds for process B, which involves the ${}^6G_J \rightarrow {}^6I_J$ transitions of Gd³⁺ and the ${}^4I_{9/2} \rightarrow {}^4F_{5/2}, {}^2H_{9/2}$ or ${}^4F_{7/2}$ transitions of Nd³⁺. These Nd³⁺ transitions also have oscillator strengths of about 5×10^{-7} .

The oscillator strengths of the transitions within the ${}^6G_{7/2} \rightarrow {}^6P_J$ or the ${}^6G_{7/2} \rightarrow {}^6I_J$ manifolds of Gd³⁺ have not been measured, but their reduced matrix elements have been calculated.⁶ The reduced matrix elements for the ${}^6G_{7/2} \rightarrow {}^6I_J$ transitions are almost a factor of 10 greater than those of the ${}^6G_{7/2} \rightarrow {}^6P_J$ transitions, yielding the expectation that under similar resonance conditions, the probability for process B should be one to two orders of magnitude greater than for process A. As described earlier, a factor of 5 was observed. The difference may be due to the quality of the energy resonance for the two processes. The Gd³⁺ oscillator strengths are calculated based on the reduced matrix elements⁶ for Gd³⁺ and Judd-Ofelt parameters for Gd³⁺ in YLiF₄.¹⁹ The total oscillator strength to all transitions ${}^6G_{7/2} \rightarrow {}^6I$ is 2×10^{-6} and for ${}^6G_{7/2} \rightarrow {}^6P_{7/2}$ it is 1.5×10^{-8} . Since there are 39 final states in 6I , each crystal field transition, on average, has an oscillator strength of $\sim 5 \times 10^{-8}$.

It is now possible to estimate the CRET transfer rates for dipole-dipole interactions in process B from Eq. (1). Using typical values of 3×10^{-7} for each transition of Nd³⁺ and 5×10^{-8} for each transition of Gd³⁺, and assuming a single perfect energy resonance with a linewidth at room temperature of 10 cm⁻¹ (spectral overlap integral=0.1), one finds a rate of $\sim 3.3 \times 10^5$ s⁻¹ for a nearest neighbor pair separated by 3.73 Å. This rate falls to $\sim 5 \times 10^4$ s⁻¹ for a next nearest neighbor pair separated by 5.15 Å. To predict what should be observed, one has to know whether the donor-donor transfer among the Gd³⁺ ions is occurring and whether it is faster than the donor-acceptor CRET rates. The results from the dynamics of process C involving a CRET from 6I to 6P suggest, based on the nearly exponential decay of 6I and rise of the ${}^6P_{7/2}$ population, that the donor-donor transfer occurs

much more rapidly than the observed CRET rate of $\sim 6 \times 10^5 \text{ s}^{-1}$ in the 2% Nd sample. If one assumes that the same is true for process A, where the CRET rates are $> 2 \times 10^7 \text{ s}^{-1}$, then the predicted rates should take into account the fact that, on average, the excited Gd^{3+} excitation spends a fraction, $4x$ (x is the fractional concentration of Nd^{3+}) of its time as one of the four nearest neighbors of Nd^{3+} . Thus, for 2% Nd, the nearest neighbor rate should be multiplied by a factor of 0.08, yielding a result of $\sim 2.7 \times 10^4 \text{ s}^{-1}$. This rate is obtained for one resonance between the $\text{Gd}^{3+} {}^6G_{7/2} \rightarrow {}^6I$ and the ${}^4I_{9/2} \rightarrow {}^4F_{5/2}, {}^2H_{9/2}$ or ${}^4F_{7/2}$ transitions of Nd^{3+} . Even if one were to assume that all Nd^{3+} transitions (12) were perfectly resonant with a transition on Gd^{3+} , which would be an extreme assumption, and if contributions from more distant pairs are added, the maximum predicted rate still would be less than 10^6 s^{-1} .

The assumption of rapid energy transfer among the Gd^{3+} donors is supported by studies of Gd^{3+} - Gd^{3+} interactions. Studies of band-to-band exciton transitions in GdCl_3 , $\text{Gd}(\text{OH})_3$, and $\text{Tb}(\text{OH})_3$ have shown that exchange interactions among nearest neighbor ions can yield resonant energy transfer rates among nearest neighbors that are as large as 10^{10} to 10^{11} s^{-1} for resonant energy transfer among Gd^{3+} ions in their ${}^6P_{7/2}$ state or Tb^{3+} ions in their 5D_4 state.²⁰ These rates correspond to the condition of resonance with homogeneous linewidths at 1.5 K of about 0.1 cm^{-1} . At room temperature, where these linewidths are $\sim 10 \text{ cm}^{-1}$, the corresponding rates would be 10^8 to 10^9 s^{-1} . Even though the exchange interaction will probably be considerably smaller in fluorides, the expectation that donor-donor transfer rates for the 6G state of Gd^{3+} should exceed $2 \times 10^7 \text{ s}^{-1}$ in GdLiF_4 seems quite reasonable.

In the limit of no energy transfer among the Gd^{3+} ions, the relaxation after the initial energy transfer from $\text{Nd}^{3+} \rightarrow \text{Gd}^{3+}$ would occur by interactions between a pair of nearest neighbors. This rate would have a maximum value of $\sim 5 \times 10^6 \text{ s}^{-1}$ if all transitions of the two ions were resonant. Even this extreme assumption falls well short of explaining the observed rate of $> 2 \times 10^7 \text{ s}^{-1}$, and the absence of fast donor-donor transfer seems unlikely. Thus, the above analysis of the experiments points strongly to the dominant role of exchange interactions in facilitating the CRET responsible for quantum splitting in $\text{GdLiF}_4:\text{Nd}$.

It would be interesting to model the full dynamics, taking into account the energy migration of the Gd^{3+} excitations in both the ${}^6G_{7/2}$ and ${}^6P_{7/2}$ states. Although this problem is a

very interesting one, it is not the subject of this paper.

VII. CONCLUSIONS

Efficient quantum splitting has been demonstrated for the Gd^{3+} - Nd^{3+} system in $\text{GdLiF}_4:\text{Nd}$ 2%. A VUV photon is absorbed by the Nd^{3+} ions, whereupon the energy is rapidly transferred to the high-lying excited states of the $4f^7$ configuration of Gd^{3+} in a time scale of nanoseconds. A rapid and effective cross-relaxation energy transfer then occurs in two steps. In the first, a Gd^{3+} ion in its metastable 6G state undergoes a transition to 6I while a Nd^{3+} ion makes a transition ${}^4I_{9/2} \rightarrow {}^4F_{5/2}, {}^2H_{9/2}$ or ${}^4F_{7/2}$ at a rate $> 2 \times 10^7 \text{ s}^{-1}$. Multiphonon relaxation effectively brings the Nd^{3+} ions down to the ${}^4F_{3/2}$ state, where they radiate the first photon. For the remaining excited Gd^{3+} ion, there occurs a second cross-relaxation energy transfer in which Gd^{3+} undergoes a transition ${}^6I \rightarrow {}^6P$ and Nd^{3+} is excited from ${}^4I_{9/2} \rightarrow {}^4I_{13/2}$. The resulting ${}^6P_{7/2}$ excitation on Gd^{3+} transfers its energy to nearly resonant states of the $4f^3$ configuration of Nd^{3+} in a time scale of about 10 – $20 \mu\text{s}$, whereby subsequent relaxation brings the population down to ${}^4F_{3/2}$ of Nd^{3+} , where the second photon is emitted. This second step appears to be less efficient than the first. The result is a quantum yield for the emission of IR photons, which has its maximum of about 1.05 ± 0.35 , under 175 nm excitation. This is considerably below the theoretical value of 2. Nonetheless, this system exhibits the highest quantum yield for quantum splitting based on cross-relaxation energy transfer and provides excellent insights into the quantum splitting process, especially with regard to an evaluation of the details of the dynamics and the mechanisms of quantum splitting. An analysis of the dynamics and the theoretical limits of the dipole-dipole contributions, leads to the conclusions that (1) there is rapid donor-donor energy migration among the Gd^{3+} ions and (2) that exchange plays the dominant role in the cross-relaxation energy transfer responsible for the quantum splitting.

ACKNOWLEDGMENTS

We gratefully acknowledge the financial support of the U.S. National Science Foundation, Grants No. 0305400 (RSM) and No. 0305449 (DAK). We also express our appreciation to K. Mishra and M. Raukas for helpful discussions and to A. Meijerink for a crystalline sample of $\text{YLiF}_4:\text{Nd}$.

¹C. Ronda, *J. Lumin.* **100**, 301 (2002).

²S. Kuck, I. Sokolska, M. Hence, M. Doring, and t. Scheffler, *J. Lumin.* **102/103**, 176 (2003).

³W. W. Piper, J. A. de Luca, and F. S. Ham, *J. Lumin.* **8**, 344 (1974).

⁴R. T. Wegh, H. Donker, K. D. Oskam, and A. Meijerink, *J. Lumin.* **82**, 93 (1999).

⁵C. Feldmann, T. Justel, C. R. Ronda, and D. U. Wiechert, *J. Lumin.* **92**, 245 (2001).

⁶P. S. Peijzel, W. J. M. Schrama, A. Meijerink, *Mol. Phys.* **102**, 1285 (2004).

⁷J. K. Berkowitz and J. A. Olsen, *J. Lumin.* **50**, 111 (1991).

⁸P. W. Dooley, J. Thogersen, J. D. Gill, H. K. Haugen, and R. L. Brooks, *Opt. Commun.* **B183B**, 451 (2000).

⁹R. T. Wegh, H. Donker, A. Meijerink, R. J. Lamminmaki, and J. Holsa, *Phys. Rev. B* **56**, 13841 (1997).

¹⁰C. Gorller-Walrand, L. Fluyt, P. Porcher, A. A. S. Da Gama, G. F. de Sa, W. T. Carnall, and G. L. Goodman, *J. Less-Common Met.*

- 148**, 339 (1989).
- ¹¹A. L. Harmer, A. Linz, and D. R. Gabbe, *J. Phys. Chem. Solids* **30**, 1483 (1969).
- ¹²J. R. Ryan and R. Beach, *J. Opt. Soc. Am. B* **9**, 1883 (1992).
- ¹³H. Kondo, T. Hirai, and S. Hashimoto, *J. Lumin.* **108**, 59 (2004).
- ¹⁴N. Takeuchi, S. Ishida, A. Matsumura, and Y. Ishikawa, *J. Phys. Chem. B* **108**, 12397 (2004).
- ¹⁵X. X. Zhang, A. B. Villaverde, M. Bass, B. H. T. Chai, H. Weidner, R. I. Ramotar, and R. E. Peale, *J. Appl. Phys.* **74**, 790 (1993).
- ¹⁶D. L. Dexter, *Phys. Rev.* **108**, 630 (1957).
- ¹⁷T. Kushida, *J. Phys. Soc. Jpn.* **34**, 1318 (1973).
- ¹⁸O. Guillot-Noel, B. Bellamy, B. Viana, and D. Gourier, *Phys. Rev. B* **60**, 1668 (1999).
- ¹⁹A. Ellens, H. Andres, M. L. H. ter Heerdt, A. Meijerink, and G. Blasse, *Phys. Rev. B* **55**, 180 (1997).
- ²⁰R. L. Cone and R. S. Meltzer, *Phys. Rev. Lett.* **30**, 859 (1973) and R. L. Cone and R. S. Meltzer, *J. Chem. Phys.* **62**, 3573 (1975).